

Rate Constant and Mechanism of the Reaction between Cl and CH₃OCl at 295 K

S. A. Carl, C. M. Roehl,[†] R. Müller,[‡] G. K. Moortgat, and J. N. Crowley*

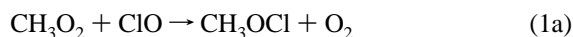
Max-Planck-Institut für Chemie, Division of Atmospheric Chemistry, Postfach 3060, D-55020 Mainz, Germany

Received: April 16, 1996; In Final Form: August 14, 1996[⊗]

The reaction between Cl atoms and CH₃OCl was investigated at 295 K in both air and N₂ bath gases at total pressures between 100 and 750 Torr by the relative rate method. The rate constant of the title reaction was found to be a factor 1.07 ± 0.02 (2σ) greater than that of Cl + C₂H₆ at room temperature and independent of pressure between 100 and 750 Torr. This yields a rate constant of $(6.1 \pm 0.6) \times 10^{-11}$ cm³ molecule⁻¹ s⁻¹. The products of the reaction were detected by FTIR and UV absorption spectroscopy. Analysis of Cl₂ and HCl products allowed branching ratios of 0.2 ± 0.1 for HCl + CH₂OCl formation and 0.8 ± 0.2 for Cl₂ + CH₃O formation to be determined. The high rate constant implies that reaction with Cl atoms is an important loss process for CH₃OCl in the polar stratosphere.

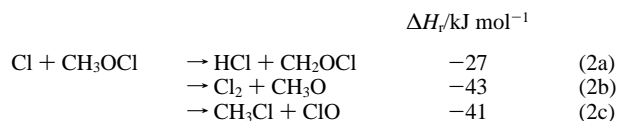
1. Introduction

The presence of high concentrations of ClO and Cl in the polar stratosphere during "ozone hole" conditions^{1,2} results in an acceleration of the rate of oxidation of CH₄ and an increasingly important role for the reaction between CH₃O₂ and ClO.³ Of the two reaction channels identified for reaction 1, one generates CH₃OCl^{4–8} with a branching ratio of close to 25% at 200 K.⁵



In previous work we have examined possible removal processes for CH₃OCl and found photolysis to be important⁹ and reaction with OH to be negligible.¹⁰

Several exothermic pathways exist for reaction 2.



The heats of reaction were calculated using $\Delta H_f(\text{CH}_3\text{OCl}) = -61$ kJ mol⁻¹ (calculated from bond additivity¹¹) and $\Delta H_f(\text{CH}_2\text{OCl}) = +125$ kJ mol⁻¹, obtained by comparison with CH₃OH and CH₂OH. ΔH_f data were taken from ref 12.

The goal of this study was to measure the rate constant for reaction 2 at 295 K and conduct a product study, at the same temperature, to determine the branching to each channel (k_{2a}/k_2 , k_{2b}/k_2 , and k_{2c}/k_2).

2. Experimental Section

The experiments designed to measure the room temperature kinetics and product formation in the reaction of Cl atoms with CH₃OCl were conducted in two separate setups, one employing Fourier transform infrared (FTIR) and the other employing ultraviolet (UV) absorption spectroscopy as analytical tools. The IR experiments involved the broad band, continuous photolysis

of suitable static gas mixtures and are designated CP-FTIR. UV absorption experiments employed pulsed laser photolysis with diode-array detection of absorption (LP-UV). These methods are described separately below.

2.1. CP-FTIR Experiments. The experimental setup consists of a cylindrical quartz reaction vessel of ca. 1.4 m length and 20 cm diameter to give a volume of 44 L. The reaction vessel is surrounded by photolysis lamps, mounted radially and parallel to the vessels' cylindrical axis, which emit between 280 and 350 nm (Philips TL 12) or at 254 nm (Philips TLUV). The lamps are surrounded by a polished aluminum sheath and provide an approximately homogeneous light flux throughout the reaction volume. Two sets of multipass optics are built into the cell, one for reflection in the IR and the other for UV wavelengths, providing absorption pathlengths of ca. 34 and 9.8 m, respectively. IR analysis was carried out using a Bomem DA-08 FTIR spectrometer operated at 0.5 cm⁻¹ resolution. A liquid-helium-cooled Cu-Ge detector was used to detect IR radiation between 450 and 3600 cm⁻¹; 256 scans were coadded over a period of ca. 7 min to provide sufficient signal/noise ratios. Detection of UV light (D₂ lamp) was with a photomultiplier tube at a single wavelength selected by a 0.25 m monochromator (1.5 nm resolution).

Gases are introduced into the reaction chamber as diluted mixtures in either Ar or N₂ through a piping system that ensures good mixing. Pressures were monitored by 1000 Torr and 100 mbar capacitance manometers; most experiments were carried out at a total pressure of 750 Torr air or N₂ and at room temperature (295 K). Calibration curves of C₂H₆, HCl, HCHO, CH₃OH, and CO were obtained by measuring optical absorbance in the 44 L cell following the dosing of 1–10 mbar amounts of accurately premixed gases (with N₂) from a 6 L glass vessel and pressurizing to 750 Torr. HCOOH, calibrated accurately in a separate experimental setup as described by Finkbeiner et al.,¹³ was determined relative to HCHO using a relative absorbance of HCOOH (1776 cm⁻¹) to HCHO (1746 cm⁻¹) equal to 1.72 at a resolution of 0.5 cm⁻¹. The CH₃OCl IR absorbance was calibrated relative to the UV absorbance at 250 nm, which in turn was converted to concentration using the cross sections given in ref 9 and the optical path length of 980 cm. The conversion of the measured absorbance to concentration was achieved by a stripping routine using calibration spectra with similar ($\pm 20\%$) absorbance. For HCl, HCHO was first stripped from the spectrum to enable between 3 and 5 HCl rotational lines to be simultaneously analyzed to determine the

* Correspondence to this author.

[†] Present address: Jet Propulsion Laboratory, California Institute of Technology, Pasadena, CA 91109.

[‡] Institut für Stratosphärische Chemie (ICG 1), Forschungszentrum Jülich GmbH, D-52425 Jülich, Germany.

[⊗] Abstract published in *Advance ACS Abstracts*, October 1, 1996.

concentration. The following IR features were used to convert absorbance to concentration: CH₃OCl, 1006 cm⁻¹; CH₃OH 1034 cm⁻¹; C₂H₆, 822 cm⁻¹; CO, 2140 cm⁻¹; HCHO, 1746 cm⁻¹; HCl, 2885 cm⁻¹; ClCHO, 1783 cm⁻¹; HCOOH, 1776 cm⁻¹. The concentrations from the IR experiments are expected to be accurate to within ±5% for stable, easily stored, and calibrated species (CH₃OCl, CH₃OH, C₂H₆, CO, HCHO), ±10% for HCl, and ±15% for HCOOH. The calibration of ClCHO was performed in situ and has an estimated accuracy of ±25%.

Cl₂ was detected by absorption at 370 nm (when Cl₂ was present in the starting mixture) or at 330 nm. The change in concentration of Cl₂ (370 nm) during photolysis of Cl₂/CH₃OCl/air(N₂) was discernible by this method but could not be accurately quantified. During the photolysis of CH₃OCl/air mixtures, Cl₂ (330 nm) could be sufficiently accurately measured to provide the branching ratio data directly. Additional details of this apparatus are found elsewhere.^{14,15}

2.2. LP-UV Experiments. The apparatus used for the LP-UV absorption study of reaction 2 comprised a parallelepiped quartz reaction/absorption cell of square internal cross section 21.1 cm² and volume 850 cm³, a pulsed laser, operating at 351 nm (XeF Eximer Laser; 25 ns pulse duration, ca. 1 nm bandwidth) used as the photolysis source, a deuterium lamp for long-path UV absorption measurements (White optics, *l* = 3.26 m), and a 0.5 m spectrograph with a gated (gate width = 65 μs), Peltier-cooled, diode-array detector with image intensifier for detection. The grating of the spectrograph was positioned to provide radiation from 235 to 350 nm over the detector face, encompassing the main UV spectral features of CH₃OCl and Cl₂. This arrangement provided a wavelength-digitized spectrum of effective spectral resolution 1.7 nm. To obtain a satisfactory signal-to-noise ratio, each recorded spectrum was derived from an average of 500 gated diode-array images and took ca. 6 s to collect. The spectrograph was calibrated for wavelength using spectral lines of a Hg pen-ray lamp.

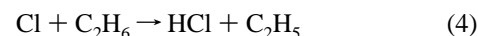
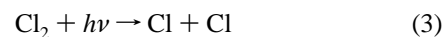
The laser beam was expanded to give approximately uniform intensity over one of the cell's rectangular faces. Cl₂ was used as the photolytic precursor for Cl atoms ($\sigma(\text{Cl}_2)_{351\text{nm}} = 1.82 \times 10^{-19}$ cm² molecule⁻¹¹²) and was admitted to the cell in a mixture of 1% Cl₂ (Linde 3.5) in N₂ (Linde 5.0). The second reactant was introduced to the cell as 1.6% CH₃OCl in Ar (with 2.8% CH₃OH impurity in CH₃OCl) from a 6 L, blackened, Pyrex bulb. Total cell pressures were constant during each experiment but were varied from experiment to experiment between 60 and 500 Torr by adding N₂ (Linde 5.0). Pressures in the cell were measured by a 1000 Torr capacitance manometer. Initial concentrations of both CH₃OCl and Cl₂ were varied between (0.5–1.4) × 10¹⁶ and (0.8–1.8) × 10¹⁶ molecules cm⁻³, respectively. Between 0.03% and 0.06% of the Cl₂ was photolyzed per laser pulse. CH₃OCl was also photolyzed to some extent by the laser ($\sigma(351\text{ nm}) = 6.3 \times 10^{-21}$ cm² molecule⁻¹⁹), but its photolytic removal was calculated to be less than 2% of its removal due to reaction with Cl. The LP-UV experiments measured the overall change in concentrations of the detectable reactant, CH₃OCl, and direct product Cl₂, together with the stable products produced by secondary reactions, namely, ClCHO and HCHO, following initiation of reaction 2 by photolysis. To easily discern changes in concentrations, particularly of Cl₂, the gaseous mixture was photolyzed 50 times (ca. 140 or 280 mJ/pulse) before a spectrum was recorded. Changes in concentrations of relevant species were extracted by computer fitting to known spectral profiles of the same resolution.

2.3. Chemicals. CH₃OCl was prepared as described previously⁹ and stored as a ca. 2% mixture in Ar in a blackened 6 L

glass bulb. C₂H₆ (Linde, 99.95%), HCl (Linde, 99.8%), Cl₂ (Linde 99.8%), and CO (Linde, 99.997%) were used without further purification. CH₃OH (Aldrich, 99.9%) was degassed prior to use. HCHO was generated by gently warming paraformaldehyde (Aldrich, 99.5%) and purified of H₂O and polymeric HCHO by passage through a glass spiral held at -100 °C, prior to dilution to 1% and storage at a low partial pressure (1–2 Torr) in a blackened glass bulb. ClCHO was generated in situ by photolysis of HCHO/Cl₂ mixtures and roughly calibrated by measuring the depletion of Cl₂ and HCHO. N₂ (Linde 99.999%) and synthetic air (Linde) were taken directly from 50 L bottles.

3. Results

3.1. Relative Rate Experiments. The room temperature rate constant for the reaction between Cl atoms and CH₃OCl was investigated using the relative rate method and FTIR detection of CH₃OCl and C₂H₆, which was used as reference gas. IR spectra of mixtures comprising Cl₂ ((2.5–3.0) × 10¹⁶ molecules cm⁻³), CH₃OCl ((1.9–3.7) × 10¹⁵ molecules cm⁻³), C₂H₆ ((2.4–3.7) × 10¹⁵ molecules cm⁻³), and N₂ or air (750 or 100 Torr) were illuminated at 280–350 nm for short periods of typically 3–5 s before IR spectra were obtained. This was repeated up to 11 times until the reactants CH₃OCl and C₂H₆ were reduced to ca. 15% of their starting concentrations. High concentrations of Cl₂ were employed to ensure that the CH₃OCl removal by photolysis was negligible compared to its reaction with Cl.



Assuming that the Cl atom production is dominated by Cl₂ photolysis and that all Cl reacts with CH₃OCl, the approximate rate of removal of CH₃OCl due to photolysis relative to reaction with Cl atoms, R_5/R_2 , is, in the absence of C₂H₆, given by

$$R_5/R_2 = J(\text{CH}_3\text{OCl})[\text{CH}_3\text{OCl}]/2J(\text{Cl}_2)[\text{Cl}_2] \quad (i)$$

Here $J(\text{CH}_3\text{OCl})$ and $J(\text{Cl}_2)$ refer to the photolysis rate constants of CH₃OCl and Cl₂, respectively. The ratio $J(\text{CH}_3\text{OCl})/J(\text{Cl}_2)$, obtained by comparing the integrated overlap of the known CH₃OCl⁹ and Cl₂ spectra¹² with the relative emission intensity of the photolysis lamps, is equal to 0.076. Assuming typical initial concentrations of 2.5 × 10¹⁵ and 3.0 × 10¹⁶ molecules cm⁻³ for CH₃OCl and Cl₂, respectively, we obtain $R_5/R_2 = 0.3\%$. In the presence of approximately equal concentrations of C₂H₆ and CH₃OCl the loss rate of CH₃OCl due to reaction with Cl is halved, and we obtain $R_5/R_2 = 0.6\%$. Photolysis of CH₃OCl is thus treated as negligible in the following analyses.

The relative rate method to acquire kinetic data does not require knowledge of the absolute concentrations of either radical or reactants but a reference compound with a well-characterized rate constant at the temperature of interest and an accurate measure of the fractional loss of both stable reactant and reference molecules. In this study, C₂H₆ was chosen as the reference molecule. The rate constant used for Cl + C₂H₆ has a recommended value¹² of $k_{\text{ref}} = (5.7 \pm 0.6) \times 10^{-11}$ cm³ molecule⁻¹ s⁻¹. The relative rate constant, k_2/k_{ref} , is derived from plots of $\ln(\text{DF}_{\text{reactant}})$ versus $\ln(\text{DF}_{\text{reference}})$, where DF is

TABLE 1: Experimental Starting Conditions for the Relative Rate Study^a

bath gas	[CH ₃ OCl] ₀	[C ₂ H ₆] ₀	[Cl ₂] ₀
air	2.46	2.43	27.2
air	2.71	2.38	29.2
air	1.93	3.69	29.2
air	3.66	2.36	29.9
N ₂	2.59	3.04	25.5
N ₂	3.19	4.18	24.3
N ₂ ^b	3.11	4.37	25.0

^a Concentrations are in units of 10¹⁵ molecules cm⁻³. ^b Carried out at 100 Torr total pressure; all other experiments were conducted at a total pressure of 750 Torr.

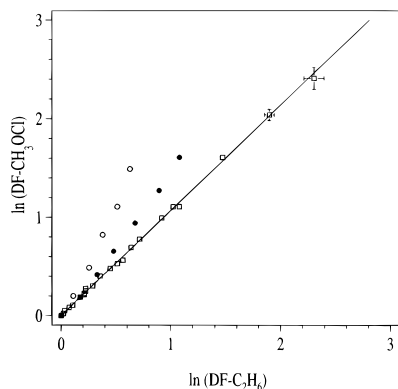


Figure 1. Relative rate study of the reaction between Cl and CH₃OCl. DF is the depletion factor and is defined in the text. Open squares, experiments in 750 and 100 Torr N₂. Circles, experiments in air. Open circles, [CH₃OCl]_i = 1.93 × 10¹⁵, [C₂H₆]_i = 3.69 × 10¹⁵ molecules cm⁻³. Solid circles, [CH₃OCl]_i = 2.71 × 10¹⁵, [C₂H₆]_i = 2.38 × 10¹⁵ molecules cm⁻³.

the depletion factor and is defined as DF = (initial concentration)/(final concentration).¹⁶ The initial concentrations for seven experiments are listed in Table 1.

Figure 1 shows such a plot for three experiments carried out in N₂ (open squares) and two carried out in air (circles). The data obtained in N₂ displays the expected behavior, with all data points lying on a single straight line with an unforced zero intercept. The error bars were derived from a propagation of the errors associated with each experimental point and are largest at high conversions where the concentrations are lowest. In contrast, the data obtained in air give strongly curved plots, with the degree of curvature varying from experiment to experiment. In air, the relative removal rate of CH₃OCl to C₂H₆ increases with time. Indeed at long times (i.e. last point of open circles) about twice as much CH₃OCl has been removed relative to C₂H₆ as compared to the N₂ experiments at similar conversion. This may imply that a further removal process for CH₃OCl apart from reaction with Cl becomes more important as the degree of conversion of reactants increases or that C₂H₆ is reformed.

In the presence of O₂ the chemistry will be dominated by formation of peroxy radicals such as C₂H₅O₂ and HO₂ and their subsequent reactions to form peroxidic and aldehydic products such as C₂H₅OOH, CH₃CHO, and H₂O₂. In such chemical systems, OH radicals are likely to be generated via photolysis of, for example, C₂H₅OOH or H₂O₂. As the reactivity of OH toward CH₃OCl is a factor 3 higher than toward C₂H₆ at 295 K,¹⁰ OH may contribute to the excess CH₃OCl removal. However, numerical simulations, incorporating a full set of reactions between the various peroxy radicals, and photolysis of photolabile species were unable to generate concentrations of OH that were sufficient to reproduce the curvature of the plots. [OH] typically remained 2 orders of magnitude less than

[Cl] and does not contribute significantly to removal of either C₂H₆ or CH₃OCl.

An examination of all four experiments in O₂ reveals that the experiments in which the ratio of CH₃OCl to C₂H₆ was lowest (open circles in Figure 1) yield the highest curvature. This may imply that the secondary loss of CH₃OCl is tied in with the enhanced C₂H₆ oxidation chemistry (RO₂ radical chemistry). Direct reaction of peroxy radicals with CH₃OCl seems however unlikely considering the negligible reactivity of HO₂ toward HOCl or CH₃O₂ to CH₃OCl.^{4,5} At present, we do not have an explanation for the unexpected behavior in C₂H₆/CH₃OCl/air.

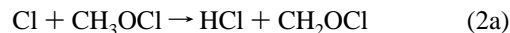
In N₂, the decay rate of CH₃OCl and C₂H₆ was enhanced by ca. 40% over that in O₂ for the same initial Cl₂ concentration and number of photolysis lamps. This is attributed to secondary generation of Cl atoms through reactions of the sort



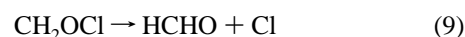
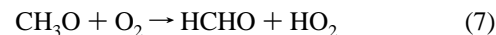
The data obtained in N₂ were fitted using a weighted least squares fitting routine and yield a result of 1.07 ± 0.02 (the error represents 2σ, statistical confidence limit). Using the recommended rate constant for Cl + C₂H₆,¹² this yields a rate constant of k₂(295) = 6.1 ± 0.6 cm³ molecule⁻¹ s⁻¹.

3.2. Broad Band Photolysis of Cl₂/CH₃OCl/Air. Product formation in the reaction between Cl and CH₃OCl was investigated by measuring the yields of several IR-active products and Cl₂ following the broad band photolysis of Cl₂/CH₃OCl/air mixtures at 750 Torr and 295 K. IR spectra were obtained prior to reaction and at various intervals following photolysis using 4 or 12 TL12 lamps. A high concentration of Cl₂ was used as a Cl atom source, and the stability of the UV detection (at 370 nm) was too low for modulation in the Cl₂ signal to be observed. This was only possible in those experiments in which CH₃OCl was photolyzed at 254 nm in the absence of initial Cl₂, enabling it to be monitored at the peak of its absorption spectrum at 330 nm (see section 3.4). Typical starting concentrations were Cl₂, (0.6–2.9) × 10¹⁶ molecules cm⁻³ (detected by UV absorption at 370 nm); CH₃OCl, (2.1–2.5) × 10¹⁶ molecules cm⁻³; air/N₂ to 750 Torr.

CH₃Cl was not detected in any experiments. As its reaction with Cl atoms is too slow to cause its removal, reaction 2c is insignificant. Analysis of the IR spectrum near 750 cm⁻¹ (C–Cl stretch) enables us to estimate an upper limit of 1% for CH₃Cl formation. The initial reaction is therefore expected to be a competition between channels 2a and 2b:



The subsequent secondary chemistry, involving CH₂OCl and CH₃O from reactions 2a and 2b, respectively, is dependent on the bath gas used. In the presence of O₂ we expect the following reactions to be important:



The products detected in air were HCl, Cl₂, HCHO, CO, and HCOOH. Both CH₃OH and CO were present at the beginning of the experiment as impurities in either the bath gas or the

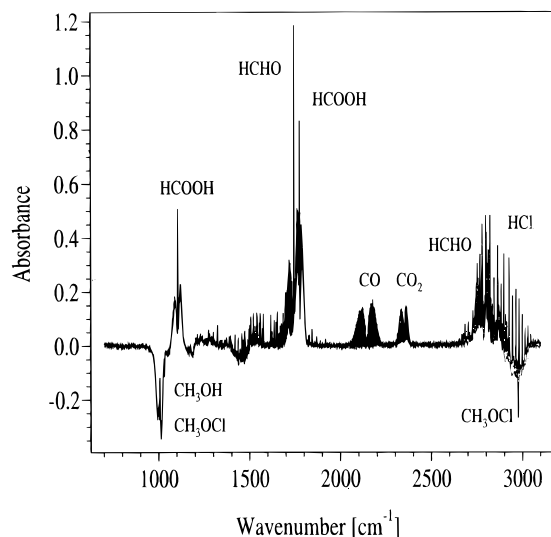


Figure 2. FTIR spectrum of products (upward pointing features) and depleted reactants (downward pointing features) following 15 s of photolysis of 2.07×10^{15} molecules cm^{-3} CH_3OCl and 0.97×10^{16} molecules cm^{-3} Cl_2 in air at 750 Torr total pressure.

CH_3OCl . Of central importance to the subsequent analyses, which compare rates of formation of products from channels 2a and 2b with the rate of loss of CH_3OCl and with each other, is that total chlorine is conserved, i.e., that there are no loss processes for these molecules that result in undetected chlorine-containing products. Therefore the chlorine balance was calculated after about 30–50% of the CH_3OCl had been depleted. In all experiments the chlorine balance was found to be close to 100% (variation between 102 and 107%), confirming that all chlorine-containing products are detected. The concentration of CH_3OCl in the darkened 44 L reactor did not change over 30 min, implying that thermal dissociation or loss at the reactor wall was negligible over the course of a photolysis experiment.

Figure 2 shows a spectrum obtained after 15 s of photolysis, in which ca. 25% of the CH_3OCl has been depleted. IR features pointing downward are reactants that are consumed; features pointing upward are products. Although $[\text{CO}_2]$ increases with time, it is not thought to be a product of the gas-phase chemistry but a result of degassing from the reactor walls under the influence of UV light.

Figure 3 shows concentration–time profiles for CH_3OCl , HCl , HCHO , CH_3OH , CO , and Cl_2 . The Cl_2 profile, although not accurately measured, shows that $[\text{Cl}_2]$ increases during the course of the experiment, providing the first qualitative confirmation that reaction 2b is taking place. Although the conversion of CH_3O to HCHO is rapid in 750 Torr of air, HCHO reacts with the concomitantly formed HO_2 , and the HCHO profile is curved from the first measurement onward. If we make the assumption that all HCHO that is lost early in the experiment has been converted to HCOOH (reaction 8), then the sum of HCHO and HCOOH should equal the total amount of HCHO generated. The HCHO , HCOOH , and $\text{HCHO} + \text{HCOOH}$ concentrations of experiment 5 (see Table 2) are plotted in Figure 4. The summed $\text{HCHO} + \text{HCOOH}$ concentration shows a linear increase until about 20 s (first four data points). After this, the removal of HCHO by Cl atoms (which does not lead to HCOOH formation) results in curvature. HCHO photolysis is negligible. The rate of increase of $\text{HCHO} + \text{HCOOH}$ over this period is equal to $(3.01 \pm 0.08) \times 10^{13}$ molecules $\text{cm}^{-3} \text{ s}^{-1}$. The rate of decay of CH_3OCl is $(3.14 \pm 0.32) \times 10^{13}$ molecules $\text{cm}^{-3} \text{ s}^{-1}$ (both errors are 2σ), yielding a branching ratio to $\text{HCHO} + \text{HCOOH}$ formation of $0.96 \pm$

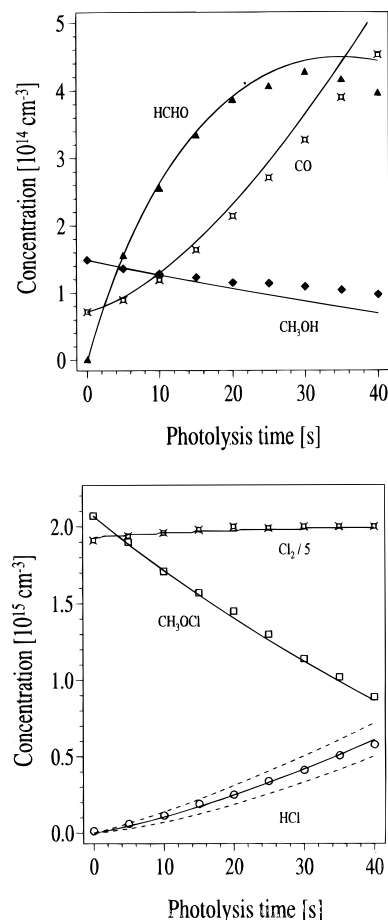
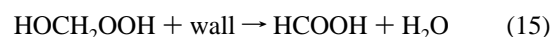


Figure 3. Concentration–time profiles of reactants and products from photolysis of $\text{Cl}_2/\text{CH}_3\text{OCl}/\text{air}$. Initial conditions are as in Figure 2. The solid lines are numerical simulations of the data and are described in the text.

0.10. The results of experiment 6 were analyzed in the same manner and yield 0.89 ± 0.10 . An average value from the two experiments is thus 0.93 ± 0.14 and provides confirmation of the quantitative conversion of CH_3OCl to HCHO as predicted by reactions 2a, 2b, 7, and 9. This suggests that the fate of CH_2OCl is adequately described by its thermal decomposition or, if CH_2OCl does not react to form HCHO , that branching to this channel is too small to effect the overall HCHO yield.

In the above, we have assumed quantitative conversion of HCHO to HCOOH , which implicitly assumes that any HOCH_2OOH generated (12b) is lost, presumably in a heterogeneous reaction (15) to give HCOOH . The following reaction scheme^{17,18} describes the formation of HCOOH :



Any HOCH_2OOH that is not converted to HCOOH means that the summed $\text{HCHO} + \text{HCOOH}$ concentration is underes-

TABLE 2: Summary of Data Obtained in the FTIR Experiments^a

	expt no.							
	2	3	4	5	6	7	8	
bath gas	N ₂	N ₂	N ₂	air	air	air	air	
10 ¹⁵ [CH ₃ OCl] _i	2.49	2.44	2.19	2.07	2.42	2.12	5.33	
10 ¹⁶ [Cl ₂] _i	2.53	2.50	0.57	0.97	2.90	0.025	0.046	
10 ¹⁴ [CH ₃ OH]	1.85	2.16	1.70	1.49	2.97	2.87	4.38	
no. lamps	12	12	12	12	4	3(Hg)	4(Hg)	
d[CH ₃ OCl]/dt (A)								
10 ¹² molec cm ⁻¹ s ⁻¹	-89.0 ±6.0(5)	-67.0 ±4.0(5)	-26.6 ±0.7(5)	-31.4 ±3.2(5)	-34.2 ±2.8(5)	-1.72 ±0.06(5)	-4.20 ±0.06(4)	
d[HCl]/dt (B) ^b								
10 ¹¹ molec cm ⁻¹ s ⁻¹				101 ±8(5)	135 ±26(5)	3.5 ±0.2(3)	5.9 ±0.7(3)	
d[HCHO]/dt (C)								
10 ¹³ molec cm ⁻¹ s ⁻¹	3.46 ±0.1(4)	3.18 ±0.3(4)	1.27 ±0.02(4)					
d[HCHO _{tot}]/dt (D) ^c								
10 ¹³ molec cm ⁻¹ s ⁻¹				3.01 ±0.08(4)	3.05 ±0.10(4)			
d[CH ₃ OH]/dt (E)								
10 ¹² molec cm ⁻¹ s ⁻¹	17.0 ±1.0(5)	13.5 ±2.0(5)	6.6 ±1.0(5)	-2.2 ±0.6(3)	-5.3 ±1.5(4)	-0.25 ±0.03(5)	-0.21 ±0.02(4)	
d[Cl ₂]/dt (F)								
10 ¹¹ molec cm ⁻¹ s ⁻¹						8.35 ±1.1(3)	27.2 ±2.6(3)	
G/A ^d				0.25	0.24			
C/A	0.39	0.46	0.49					
D/A				0.96	0.89			
E/A	0.19	0.20	0.25					
B/F						0.12	0.14	

^a Numbers in parentheses are the number of points through which the slope was determined. Negative sign implies depletion; errors are 2σ statistical uncertainty. ^b Not corrected for production via Cl + CH₃OH. ^c HCHO_{tot} = HCHO + HCOOH. ^d HCl production rate corrected for Cl + CH₃OH.

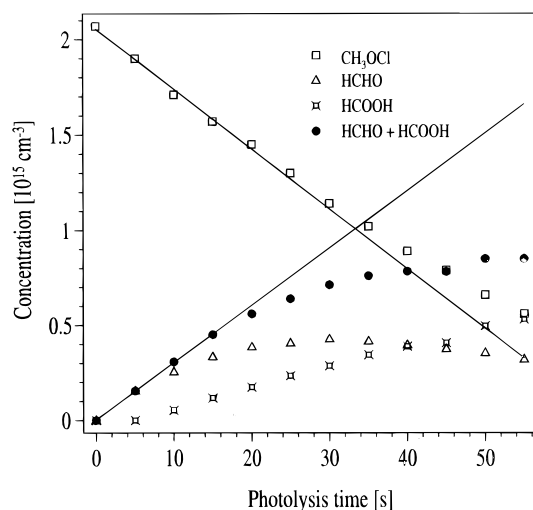
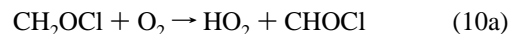


Figure 4. Concentration–time profiles of CH₃OCl, HCHO, HCOOH, and HCHO + HCOOH in air. The solid lines are initial slopes of the HCHO + HCOOH production rate and the CH₃OCl removal rate.

timated. The IR spectra were inspected for the presence of HOCH₂OOH by comparison with the published spectra (feature at ca. 1150 cm⁻¹) of Su et al.¹⁹ Although no evidence for HOCH₂OOH was found, the feature at 1150 cm⁻¹ is weak, broad, and in a region where CH₃OH and HCOOH have very strong interfering absorptions. For this reason we cannot rule out its presence and prefer to quote the summed HCHO + HCOOH concentration and the 93% conversion of CH₃OCl to HCHO as a lower limit.

In reaction 9 we assume that the fate of CH₂OCl in air is thermal decomposition. This assumption is based on an upper limit to the thermal lifetime of a similar radical, CH₂OOH, which decomposes within 20 μs in 50 Torr of He at 205 K²⁰ and

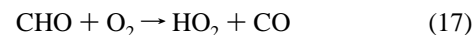
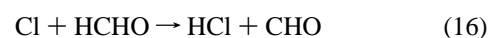
consideration of the energetics of possible pathways for reaction with O₂:



Reaction 10a is expected to be highly endothermic, whereas reaction 10b is calculated as exothermic by greater than 100 kJ/mol. However, the fate of ClOO at 295 K and 760 Torr is rapid decomposition to Cl and O₂, and thus the direct thermal decomposition of CH₂OCl and reaction 10b give the same net result. In the following analyses we therefore assume that CH₂OCl decomposes immediately to HCHO and Cl.

Rates of formation of products relative to the removal rate of CH₃OCl are listed in Table 2 along with the starting conditions for five experiments (nos. 2–6) carried out in air and N₂. The rate of HCl formation relative to CH₃OCl decomposition had to be corrected for the initial presence of CH₃OH. In all experiments, CH₃OH impurities were between 5 and 10% of the CH₃OCl concentration. As CH₃OH is removed only by reaction with Cl and is not generated in the air system, the correction was simply achieved by subtracting the initial CH₃OH decay rate from the initial HCl production rate. The relative rate of production of HCl to loss of CH₃OCl (Table 2, experiments 5 and 6) is then 0.25 ± 0.04, where the errors are propagated from 2σ errors in d[CH₃OCl]/dt, d[CH₃OH]/dt, and d[HCl]/dt as given in Table 2.

Figure 3 shows that, in experiments carried out in air, CO is formed at low conversion of CH₃OCl. The CO is formed in the secondary reaction between Cl and HCHO in air,



and indicates that secondary chemistry may influence even our first measurement point. This makes it very difficult to measure HCl before secondary chemistry contributes to its formation. Assuming an initial concentration of CH₃OCl of 2.5×10^{15} molecules cm⁻³, a minimum conversion of 5% of the CH₃OCl is needed to obtain a usable signal of HCl. This simply reflects the low branching ratio to HCl formation. That is, a 10% branching ratio and 5% conversion of CH₃OCl give ca. 1×10^{13} molecules cm⁻³ of HCl, which is close to the detection limit in our setup. This problem is compounded by the high reactivity of Cl to HCHO, which is formed as a major product via reaction 7 and which forms HCl with 100% efficiency. Thus, 5% conversion of CH₃OCl implies a HCHO concentration roughly 5% that of CH₃OCl. This will scavenge ca. 5% of subsequent Cl atoms and contribute 50% of HCl at this early stage of the reaction. Use of significantly higher concentrations of CH₃OCl to avoid such effects results in saturation of the IR signal. For these reasons, the results were checked by numerical simulation of a model containing the reactions described in the body of the text.

3.3. Numerical Simulations of Product Formation in Air.

The numerical simulations²¹ were carried out primarily in order to assess to what extent HCl formation is influenced by the reactions of HCHO and CH₃OH with Cl at short reaction times.

The rate of photolysis of Cl₂, $J(\text{Cl}_2)$, is required in such simulations and was determined by monitoring with FTIR the rate of formation of HCl and depletion of C₂H₆ when static Cl₂/C₂H₆ mixtures were photolyzed in air. The following reactions are expected to take place:



The measured rate of formation of HCl or depletion of C₂H₆ is then given by $d(\text{HCl})/dt = -d(\text{C}_2\text{H}_6)/dt = 2J(\text{Cl}_2)[\text{Cl}_2]_i$. The initial Cl₂ concentration can be determined accurately by UV absorption spectroscopy. The HCl and C₂H₆ profiles thus obtained were slightly curved due to the changing rate of Cl atom production as the Cl₂ concentration is depleted. Initial slopes could be determined only with limited accuracy, and it was necessary to model the HCl formation and C₂H₆ decay using a numerical simulation initiated with the above [Cl₂]_i and [C₂H₆]_i concentrations. On the basis of HCl production, $J(\text{Cl}_2)$ was found to be $(1.27 \pm 0.06) \times 10^{-3} \text{ s}^{-1}$ when the lamps were switched on for a nominal 3 s photolysis period. The value obtained by analyzing the C₂H₆ profile was $(1.13 \pm 0.06) \times 10^{-3} \text{ s}^{-1}$. For 5 s photolysis periods, values of $(2.01 \pm 0.12) \times 10^{-3} \text{ s}^{-1}$ (HCl production) and $(1.86 \pm 0.15) \times 10^{-3} \text{ s}^{-1}$ (C₂H₆ decay) were obtained. The different values for $J(\text{Cl}_2)$ for 3 and 5 s photolysis periods are due to flickering of the lamps when switching on. The errors given in the $J(\text{Cl}_2)$ value represent only the goodness of the fit to the HCl and C₂H₆ profiles. A more realistic error includes the expected uncertainty in calibration and measurement of Cl₂, C₂H₆, and HCl and approaches 20%. Although of negligible influence, the photolysis rates of CH₃OCl and HCHO, calculated using known absorption cross sections and quantum yields, were included in the numerical simulations.

The solid lines in Figure 3 show the result of fitting the experimental CH₃OCl and HCl profiles to a reaction scheme consisting of reactions 2a, 2b, 3, 5, 7, 9, and 11–17). The simultaneous fit to the CH₃OCl and HCl data returns a branching ratio of k_{2a}/k_2 of 0.18 ± 0.02 , i.e. 18% branching to HCl

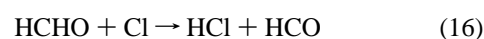
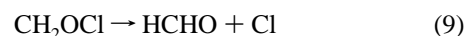
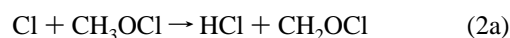
formation. This is lower than the value of 24% obtained using initial slopes (Table 2), as the formation of HCl via reactions of Cl with HCHO and CH₃OH is rigorously taken into account. In such simulations, the decay rate of CH₃OCl is controlled by the available Cl atom concentration. This not only is governed by the photolysis rate constant of Cl₂, $J(\text{Cl}_2)$, and the Cl₂ concentration but also depends on the branching ratio to CH₂OCl formation, which results in secondary Cl atom production. Therefore not only k_{2a}/k_2 and k_{2b}/k_2 but also $J(\text{Cl}_2)$ was optimized. The best fit value of $J_{\text{fit}}(\text{Cl}_2)$ was $1.65 \times 10^{-3} \text{ s}^{-1}$. This is lower than but within the uncertainty of our independent $J(\text{Cl}_2)$ determinations. In the present model, HCHO is generated in each reaction of Cl with CH₃OCl and is therefore not very sensitive to branching ratio. The HCHO and CO profiles are however adequately reproduced using this mechanism and branching ratio of 0.18 to HCl formation. To test the sensitivity of the data to changes in branching ratio, values of k_{2a}/k_2 of 0.1 and 0.3 were fixed, and the $J(\text{Cl}_2)$ necessary to fit the CH₃OCl data was varied. The results of these simulations are shown in Figure 3 as dotted lines ($k_{2a}/k_2 = 0.1$, $J_{\text{fit}}(\text{Cl}_2) = 1.8 \times 10^{-3} \text{ s}^{-1}$) and dashed lines ($k_{2a}/k_2 = 0.3$, $J_{\text{fit}}(\text{Cl}_2) = 1.6 \times 10^{-3} \text{ s}^{-1}$) enveloping the HCl profile.

3.4. Photolysis of CH₃OCl/Air at 254 nm. Experiments in which mixtures of CH₃OCl in air were photolyzed at 254 nm were carried out with the aim of measuring simultaneously the rate of generation of both Cl₂ and HCl. The advantage of this method is that the rates of formation of the HCl and Cl₂ do not have to be related to the loss of CH₃OCl and that the modulation of the Cl₂ signal at 330 nm is particularly strong as there is no offset due to a large initial concentration as in the experiments described above. However, as CH₃OCl absorbs at 330 nm, its depletion contributed to the change in absorbance upon photolysis. Therefore CH₃OCl profiles measured in the IR were used to correct the absorbance measurements at 330 nm before they could be converted to Cl₂ concentrations.

Table 2 lists the initial slopes for HCl and Cl₂ formation from experiments 7 and 8. The averaged ratio, $d(\text{HCl})/d(\text{Cl}_2)$, for the first three data points (200 s) is 0.14. After this period the ratio increases as Cl begins to react with HCHO and generate secondary HCl. The initial value of $d(\text{HCl})/d(\text{Cl}_2)$ corresponds to a branching ratio for $k_{2a}/k_2 = 0.12 \pm 0.03$ or $k_2/k_2 = 0.88 \pm 0.20$.

3.5. CP-FTIR and LP-UV Experiments in N₂. In the absence of O₂ as a scavenger for CH₃O a complex radical chemistry evolves. The chemistry may be divided into two phases: an initial phase where HCHO is generated rapidly relative to HCl and a second phase where this behavior is reversed. At the onset of the second phase, CO and ClCHO are formed. If the reaction is allowed to proceed further, only HCl and CO₂ remain as products, which are unreactive toward Cl.

The observed end products (after ca. 50% depletion of CH₃OCl) in the IR experiments were Cl₂, HCl, HCHO, CH₃OH, ClCHO, and CO. Concentration–time profiles of these species are shown in Figure 5. The following mechanism qualitatively describes their formation:



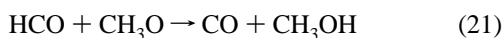


Figure 5 shows how the HCl and ClCHO production rates increase significantly after ca. 20 s of photolysis. At this point the CH₃OCl depletion rate increases and the net production of Cl₂ is reversed as phase 2 sets in. At the same time the formation of HCHO is partially offset by its removal by reaction with Cl atoms, which leads, via an unknown secondary reaction, to CO generation (reaction 21 has a very large rate constant, but the fate of HCO is likely to be dominated by (20)).

In Table 2 are listed the rates of change of concentration for the CP-IR experiments in N₂. Unfortunately, the correction to d(HCl) as applied in the experiments in air cannot be undertaken here, as CH₃OH is formed in reaction 19 and the d(HCl)/d(CH₃OCl) analysis is not appropriate. Some sensitivity to the branching ratio is expected to be found in the relative rates of HCHO production and CH₃OCl depletion. According to the above mechanism, the branching ratio k_{2b}/k_2 is given by

$$k_{2b}/k_2 = -2[(d(\text{HCHO})/d(\text{CH}_3\text{OCl}) - 1)] \quad (\text{ii})$$

at low conversion of CH₃OCl. However, the measured value of d(HCHO)/d(CH₃OCl) is equal to 0.45 (Table 2) and leads to a branching ratio in excess of unity.

The CH₃OH profile should also reflect branching to channel 2b in this system. The branching ratio k_{2b}/k_2 is given by

$$k_{2b}/k_2 = 2d(\text{CH}_3\text{OH})/d(\text{CH}_3\text{OCl}) \quad (\text{iii})$$

From Table 2 we see that d(CH₃OH)/d(CH₃OCl) = 0.2, resulting in a value of k_{2b}/k_2 of 0.4.

Thus we derive a branching ratio of about 0.4 from the CH₃OH growth curve, which is inconsistent with the observation of Cl₂ formation in the N₂ system, and derive branching ratios in excess of unity from the HCHO profile. This leads us to conclude that the above mechanism describing the reactions of CH₃O and CH₂OCl in N₂ may be incomplete. We come back to this point later.

In the LP-UV experiments Cl₂ could be accurately measured. Figure 6 shows a series of spectra obtained from a single, static gaseous mixture that had been exposed to 10 sets of 40 photolysis pulses (every alternate spectrum has been omitted for clarity). Absorption below 260 nm is approximately representative of [CH₃OCl], whereas absorption around 330 nm is approximately representative of [Cl₂]. The initial spectrum was taken before the first laser pulse and therefore shows initial absorption due to Cl₂ and CH₃OCl. The later spectra, taken at 40 pulse intervals, increasingly show structure above 280 nm due to formation of HCHO. ClCHO was also detected in these experiments; it has a broad, structured absorption with a maximum, in the near UV, around 260 nm,²² but is difficult to discern in Figure 6. Qualitatively, one may observe an overall increase in Cl₂ concentration with the number of laser pulses and a decrease in CH₃OCl concentration. These spectra were numerically fitted to known absorption profiles of the four molecules mentioned above^{9,22-24} to obtain their absolute concentrations. Concentrations of CH₃OCl, Cl₂, ClCHO, and HCHO plotted as a function of number of photolysis pulses are shown in Figure 7. The slopes of plots, such as those shown in Figure 7, derived from experiments where competition for Cl atoms from HCHO and CH₃OH is observed to be negligible, may be taken to represent the changes in concentrations of Cl₂, CH₃OCl, and HCHO for a single laser pulse.

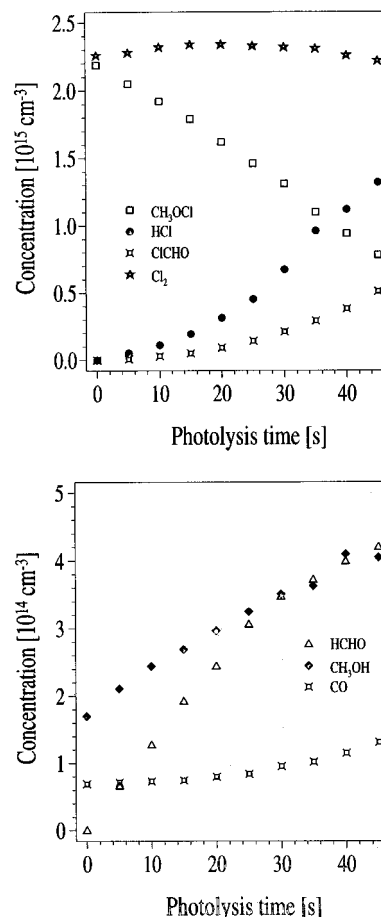


Figure 5. Concentration–time profiles of CH₃OCl, HCHO, Cl₂, HCl, ClCHO, CH₃OH, and CO in N₂ (experiment 4). Initial concentrations are given in Table 2.

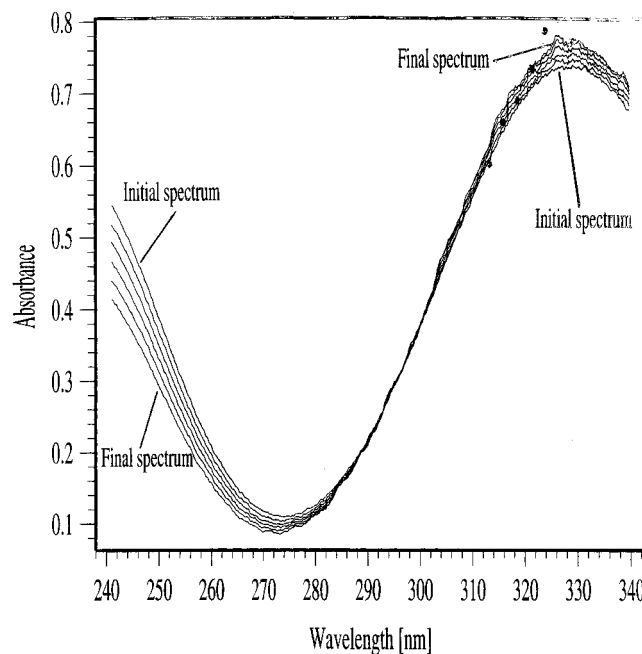


Figure 6. UV spectra collected at intervals of 80 photolysis pulses during a LP-UV experiment. The structure above 270 nm in the latter spectra is due to absorption by HCHO.

The results from several experiments are listed in Table 3 along with initial concentrations of CH₃OCl and Cl₂. A simple analysis is carried out in which the initial rate of CH₃OCl removal is compared to the initial rate of production of Cl₂. A

correction is applied to take into account Cl_2 removed by laser photolysis, and the branching ratio is, to a first approximation, given by

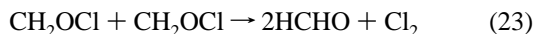
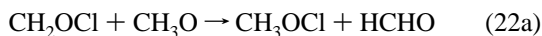
$$k_{2b}/k_2 = (\Delta(\text{Cl}_2) + \Delta(\text{CH}_3\text{OCl})/2)/\Delta(\text{CH}_3\text{OCl}) \quad (\text{iv})$$

yielding an average branching ratio of $k_{2b}/k_2 = 0.78 \pm 0.10$.

As in the FTIR experiments, the HCHO data show low $\Delta(\text{HCHO})/\Delta(\text{CH}_3\text{OCl})$ ratios, in this case consistently close to 30%. Use of eq ii then yields branching ratios much in excess of unity and in conflict with the Cl_2 data.

The measurements of Cl_2 production in the experiments carried out in N_2 support the conclusion of a high branching ratio (close to 80%) to reaction 2b. The complexity of the secondary chemistry in the absence of O_2 renders numerical modeling of the concentration profiles gained in the LP-UV and CP-FTIR experiments very difficult and imprecise. Experiments were carried out in air in the LP-UV setup but were beset by an experimental artifact that resulted in a chlorine balance of between 120 and 200%, depending on the initial O_2 partial pressure. We do not have an adequate explanation for this behavior but cannot rule out that the high intensity of the laser light may result in the generation and photodesorption of chlorine originating from a reservoir species from the reactor walls.

Up to now we have based our analysis on the assumption that CH_2OCl formed in reaction 2a decomposes thermally to yield Cl and HCHO . We note however that in the N_2 experiment the CH_3OH and HCHO yields are then not consistent with a branching ratio of 0.8 in channel 2b that is derived from the $d(\text{HCl})/d(\text{CH}_3\text{OCl})$ and $d(\text{HCl})/d(\text{Cl}_2)$ ratios in air and the $d(\text{HCl})/d(\text{Cl}_2)$ ratio in N_2 . Some of this may conceivably be due to losses of CH_3O at the reactor surface, and the different $\text{HCHO}/\text{CH}_3\text{OCl}$ ratios obtained in the CP-IR (0.45) and LP-UV experiment (0.3) may simply reflect the different surface to volume ratios and pressures used in the two reactors. In the N_2 system, we might also regard the perturbed CH_3OH and HCHO profiles as stemming from reactions that interfere with the CH_3O self-reaction. If we assume that CH_2OCl is thermally stable, we expect the following reactions to be fast:



Using a typical Cl_2 concentration of about 1×10^{16} molecules cm^{-3} and a typical alkyl radical + Cl_2 rate constant (1×10^{-12} cm^3 molecule $^{-1}$ s^{-1}), we derive a loss rate of 1×10^4 s^{-1} for CH_2OCl or a chemical lifetime of about 100 μs due to reaction 24, which dominates over the radical-radical reactions (22, 23) in the CP-IR experiments. In the pulsed LP-UV experiments the peak radical densities will be higher and the flux through reactions 22 and 23 will increase relative to reaction 24. This is a possible explanation for the different $d(\text{HCHO})/d(\text{CH}_3\text{OCl})$ ratios in the two experiments. With the exception of reaction 24 all of these reactions result in HCHO formation and cannot account for our observations of low HCHO yields. Should reaction 24 take place, the branching ratio of about 78% to Cl_2 formation that was derived from the $\Delta(\text{Cl}_2)/\Delta(\text{CH}_3\text{OCl})$ data in the LP-UV experiments in air is a lower limit to the real value.

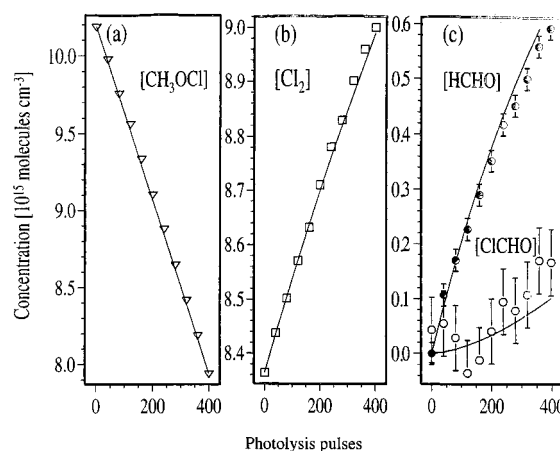
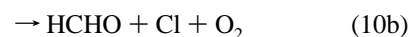
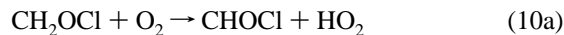


Figure 7. Concentration profiles of reactants and products during a LP-UV experiment.

On the other hand, a survey of the IR spectra close to 750 cm^{-1} ($\text{C}-\text{Cl}$ stretching region) revealed absorption due only to ClCHO , and we have no evidence for ClCH_2OCl formation.

In air a thermally stable CH_2OCl could react with O_2 :



As already discussed, reaction 10a is endothermic and reaction 10b has the same net effect as thermal dissociation of CH_2OCl . Reaction 10c forms a peroxy radical, which would probably react with HO_2 to form a peroxide:



This would however not affect our analysis of CH_3OCl , HCl , or Cl_2 profiles.

3.6. Summary of Branching Ratio Data. The results obtained provide a fairly consistent picture of product formation in the reaction between Cl and CH_3OCl and show that HCl formation via H atom abstraction is the minor channel. Analysis of the data obtained by photolysis of $\text{Cl}_2/\text{CH}_3\text{OCl}/\text{air}$ mixtures was carried out by comparing initial rates of HCl formation to decay rates of CH_3OCl . A result of k_{2a}/k_2 of 0.25 is thus obtained. This value is corrected downward to about $k_{2a}/k_2 = 0.18$ using numerical simulations that account for HCl formation via the reaction between Cl and HCHO . Analysis of total carbonyl bond containing molecules (HCHO and HCOOH) was carried out and showed that CH_3OCl is stoichiometrically converted to HCHO in air. For experiments in which CH_3OCl was photolyzed at 254 nm in air, Cl_2 and HCl profiles could be analyzed to give the ratio k_{2a}/k_{2b} directly. This was found to be 0.13 and yields branching ratios of $k_{2a}/k_2 = 0.12$ and $k_{2b}/k_2 = 0.88$. In the LP-UV experiments in N_2 , Cl_2 profiles could be analyzed to give a branching ratio of k_{2b}/k_2 of 0.78.

Although the measurements do constrain the possible branching ratio, the uncertainties in the data and in the interpretation of the chemical mechanism do not allow us to give a precise branching ratio for reaction 2, and we prefer to quote approximate values of k_{2a}/k_2 and k_{2b}/k_2 of 0.2 ± 0.1 and 0.8 ± 0.2 , respectively.

We note that a branching ratio of $k_{2a}/k_2 = 0.2$ yields a site-specific rate constant of about 1.2×10^{-11} cm^3 molecule $^{-1}$ s^{-1}

TABLE 3: Results of the LP-UV Experiments in N₂^a

expt	[CH ₃ OCl] _i /10 ¹⁶	[Cl ₂] _i /10 ¹⁶	Δ[CH ₃ OCl]/10 ¹²	Δ[Cl ₂]/10 ¹²	(d[HCHO]) _i /10 ¹²	k _{2b} /k ₂
1	1.0	1.4	-10.6 ± 0.1	3.08 ± 0.04	3.40 ± 0.40	0.79
2	0.61	1.6	-10.3 ± 0.3	2.63 ± 0.07	3.39 ± 0.35	0.76
3	0.98	0.94	-5.90 ± 0.04	1.89 ± 0.08	2.21 ± 0.35	0.82
4	1.0	1.5	-6.57 ± 0.06	1.82 ± 0.03	1.89 ± 0.07	0.78
5	1.0	0.84	-5.43 ± 0.05	1.72 ± 0.04	1.66 ± 0.10	0.82
6	0.46	1.8	-9.98 ± 0.03	1.71 ± 0.10	3.65 ± 0.04	0.67
7	1.3	1.4	-7.00 ± 0.10	2.35 ± 0.05	2.67 ± 0.30	0.84
8	1.4	1.2	-6.43 ± 0.05	1.88 ± 0.03	2.50 ± 0.10	0.79

^a All concentrations in units of molecules cm⁻³. Branching ratios (*k*_{2b}/*k*₂) derived from analysis of Cl₂ growth.

for the H atom abstraction. Although lower than the rate constant for Cl + CH₃OH (5.4×10^{-11} cm³ molecule⁻¹ s⁻¹,¹² it is comparable to that for Cl + CH₃ONO (9.5×10^{-12} cm³ molecule⁻¹ s⁻¹²⁵ and larger than that for CH₃ONO₂ (2.6×10^{-13} cm³ molecule⁻¹ s⁻¹²⁶).

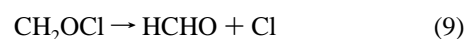
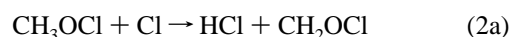
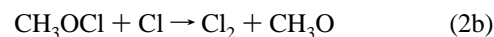
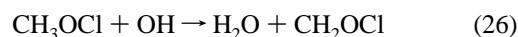
In our previous study of the reaction between OH and CH₃OCl¹⁰ we concluded, on the basis of measured Arrhenius parameters, that the reaction proceeded via H atom abstraction, but did not rule out the possibility of Cl atom abstraction. The present results show deactivation of the H-site and a highly reactive Cl-site for the Cl reaction and may add support for a Cl abstraction and formation of HOCl in the OH + CH₃OCl reaction. Further evidence for a highly deactivated H-site is provided by a recent study²⁷ of the OH + CH₃OCl reaction, in which HOCl was measured by mass spectrometry and identified as the major product (ca. 80% branching to HOCl + CH₃O).

4. Stratospheric Chemistry of CH₃OCl

The interest in CH₃OCl as a species that is expected to be formed in the polar stratosphere lies in the fact that it contains a chlorine atom and may therefore conceivably take part either in catalytic O₃ destroying cycles, as does another hypochlorite, HOCl, or it may represent a relatively stable sink for chlorine, which could lead to lower O₃ depletion rates.

Under the conditions in which the formation of CH₃OCl is maximized in the polar stratosphere (low O₃, high ClO) Cl concentrations are concomitantly high, and the high rate constant for Cl + CH₃OCl makes the reaction between Cl and CH₃OCl a potentially important removal process for CH₃OCl that can compete with photolysis. We assume, as for the reaction between Cl atom and Cl₂O, which also has a large room temperature rate constant (9×10^{-11} cm³ molecule⁻¹ s⁻¹¹²) and forms Cl₂, that the rate constant will display at most a weak temperature dependence, and we use the room temperature result from this study to examine the importance of the reaction between Cl and CH₃OCl in the stratosphere, where temperatures may be as low as 185 K. *J*-values for CH₃OCl are close to 5×10^{-5} s⁻¹ at zenith angles of between 80° and 90° and 100 mbar, giving a lifetime of ca. 4 h with respect to photodissociation.⁹ Equal importance for the reaction between Cl and CH₃OCl is therefore achieved when Cl atom concentrations of 1×10^6 are reached. In the following modeling study we show that removal by reaction with Cl atoms contributes to removal of CH₃OCl. This is in contrast to HOCl, which reacts relatively slowly with Cl atoms.¹²

4.1. Chemical Box Model Study. We employ a chemical box model^{3,28–30} including a comprehensive set of stratospheric gas-phase and heterogeneous reactions on NAT and ice surfaces as well as the hydrolysis of ClONO₂ and N₂O₅ on liquid sulfate aerosol. For the present study, we have included the formation of CH₃OCl via reaction 1 and the loss of CH₃OCl via refs 9, 10, this work)



For the computation of the photolysis rates we use an updated version of the scheme by Lary and Pyle³¹ using a typical Antarctic ozone profile and a surface albedo of 0.8. Rate constants and absorption cross sections are taken from DeMore et al.¹²

The formation of nitric acid trihydrate (NAT) and ice particles in the model depends on the prevailing temperatures and the partial pressures of HNO₃ and water vapor. The total surface area of the NAT and ice particles was computed assuming a monodisperse aerosol distribution as in earlier studies.³ The observed denitrification and dehydration³³ in the polar vortex are taken into account; it is assumed that about one-quarter of the initial HNO₃ and 2 ppm H₂O remain after the PSC (polar stratospheric cloud) period.

We simulate the typical chemical history of an air mass at polar latitudes in the stratosphere over austral winter and spring, similar to a recent study,²⁹ but for higher altitudes. Here, the air parcel is initialized on June 1 at 15 hPa (650 K), and it is assumed that it descends to 80 hPa (425 K) until the end of October in accordance with the descent indicated by observations of CH₄ in the Antarctic vortex by the HALOE.³⁴ A linearly decreasing temperature during polar night and the temperature increase after polar sunrise are estimated from measurements made at the Neumayer station (71°S, 8°W) [H. Gernandt, personal communication]. As well as approximate temperature variations with longitude caused by dynamical processes in the Antarctic vortex,³⁵ a temperature variation with an amplitude of 5 K and a period of 7 days is superimposed on the adopted temperature trend. The modeled air parcel is assumed to circulate within the polar vortex at an average latitude of 75°S with sinusoidal variations in latitude, with an amplitude of 10° and a period of 5 days to account approximately for deviations from purely zonal flow in the vortex region.

Initial values of O₃, CH₄, HCl, H₂O, NO, and NO₂ are taken from HALOE observations³³ at 48°S and 85°E, on June 2, 1993, when HALOE sounded early vortex conditions in austral winter at midlatitudes during a Rossby-wave breaking event. Values for total inorganic chlorine, Cly, are derived from the interrelationship of Cly with CH₄,³⁶ values for reactive nitrogen, NO_y, are derived from the interrelation of NO_y with N₂O.³¹ The initial values are O₃ = 5.0 ppmv, HNO₃ = 5.3 ppbv, H₂O = 4.5 ppmv, CH₄ = 1.0 ppmv, HCl = 1.6 ppbv, ClONO₂ = 1.2 ppbv, NO = 2.0 ppbv, and NO₂ = 4.0 ppbv.

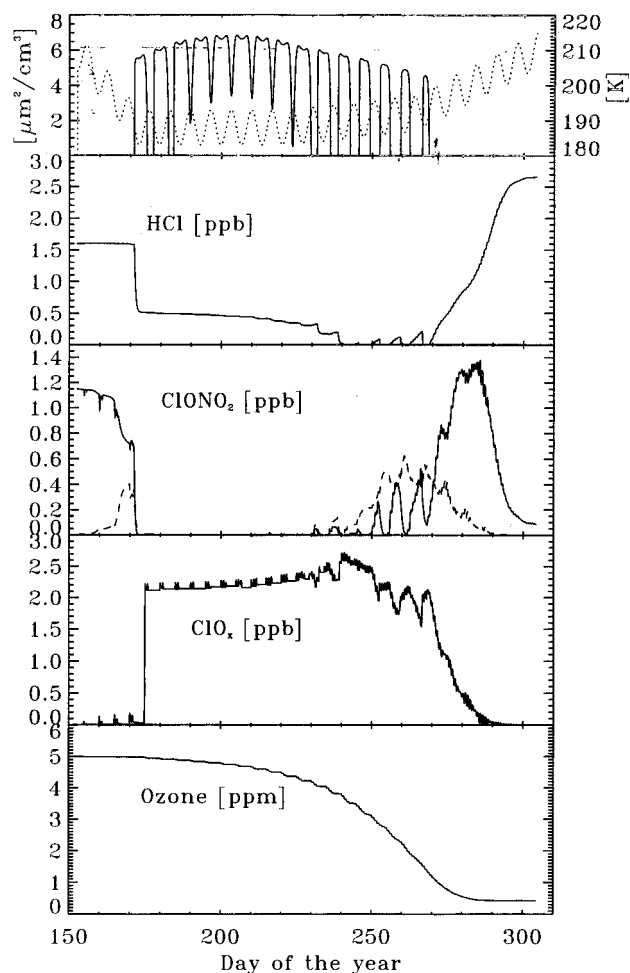


Figure 8. Adopted temperature history (dotted line) and NAT surface area (in $\mu\text{m}^2/\text{cm}^3$) (solid line) over the model period from June 1, 1993, to October 31, 1993 (upper panel). The second panel shows the HCl mixing ratio, the third panel the mixing ratios of ClONO_2 (solid line) and HOCl (dashed line), the fourth panel the mixing ratio of ClO_x ($\text{ClO}_x = \text{Cl} + \text{ClO} + 2\text{Cl}_2\text{O}_2$) over the model period, and the lowest panel the mixing ratio of ozone.

For the temperature development assumed here, NAT particles exist in the model for the period from mid June to the end of September (Figure 8), in good agreement with a climatology of PSC occurrence in the polar regions.³⁴ With the first occurrence of PSCs HCl is rapidly titrated against the available ClONO_2 and HOCl via reactions catalyzed by NAT surfaces and is converted to active chlorine ClO_x ($=\text{Cl} + \text{ClO} + 2\text{Cl}_2\text{O}_2$). The further decrease of HCl is much slower and is controlled by the production rate of HOCl and ClONO_2 ;²⁷ therefore it takes more than 2 months before the HCl is completely activated (Figure 8).

When HCl has been almost completely removed in the model (mid August, Figure 8), it can no longer act as a sink for OH, and thus, while HNO_3 is still sequestered in PSCs, OH levels increase dramatically. During this period, ozone depletion also gains momentum, and, as a consequence, extremely high Cl atom concentrations occur.^{29,37} For both reasons, increasing OH and increasing Cl radical concentrations, the methane oxidation chain is strongly enhanced in late September and, consequently, the peak mixing ratios of CH_3OCl of about 6 pptv are reached (Figure 9).

The high Cl concentrations, however, result in formation of HCl via reaction with CH_4 . Indeed, after the last PSC event at the end of September, HCl increases rapidly from 0 to 2.7 ppbv over about a month. Such a rapid HCl buildup is

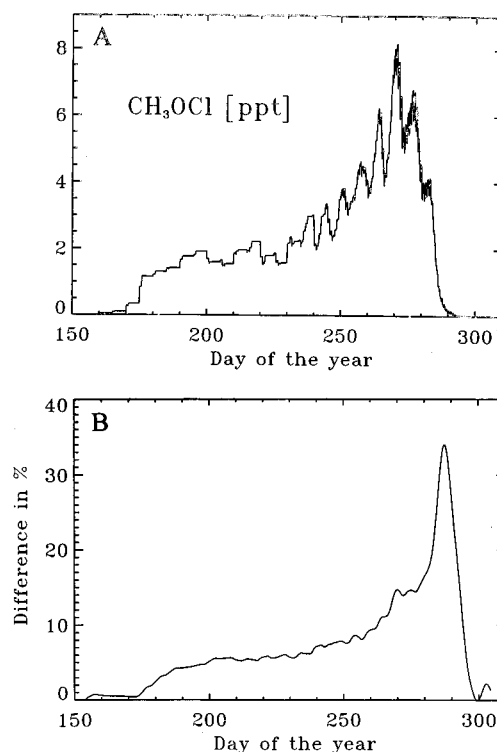
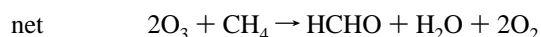
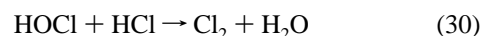
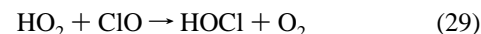
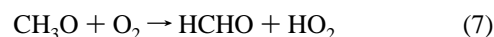
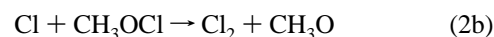
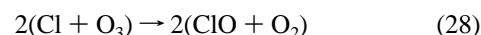


Figure 9. (A) Temporal development of the calculated CH_3OCl mixing ratios. (B) Percentage difference (smoothed with a 4 day filter) between the CH_3OCl mixing ratios of a model run neglecting the title reaction and a run with the full reaction scheme.

the typical pattern of chlorine deactivation for Antarctic conditions.^{29,36}

To investigate the atmospheric significance of the title reaction, we performed a model calculation in which it was neglected as a loss process for CH_3OCl . Under this assumption up to 35% higher mixing ratios of CH_3OCl are computed (Figure 9), showing that reaction 2 is indeed a significant loss channel for CH_3OCl .

We have shown that the reaction of CH_3OCl with Cl atoms releases photolabile Cl_2 and that this reaction can take place in the polar stratosphere. We can thus write the following catalytic O_3 destruction sequence in which HCl formed in the first step of the CH_4 oxidation (27) is activated by a heterogeneous reaction with HOCl (30), which is formed in subsequent HO_x chemistry.³



The net reaction is thus identical to that obtained when the reaction between CH_3O_2 and ClO yields the products CH_3O

and ClOO, as assumed in the original modeling study of Crutzen et al.³ and confirmed in this laboratory.⁴ Indeed the net reaction above is also identical to that obtained when CH₃OCl is photolyzed to CH₃O + Cl.⁹

Therefore, as the loss processes for CH₃OCl are relatively fast and not rate limiting in any of the catalytic reaction schemes (e.g. above) that can be written, its formation in reaction 1 should not significantly alter the role of the Cl atom initiated methane oxidation in modifying the O₃ depletion mechanism proposed by Crutzen et al.³

This assumption could be confirmed in the box model study, which returned practically unaltered O₃ loss rates with and without reaction 2. Indeed, further test calculations (not shown) indicate that even completely neglecting the formation of CH₃OCl in reaction 1b (as in ref 3) does not affect the calculated ozone loss, as already suggested by Crowley et al.⁹

5. Conclusions

The reaction between Cl and CH₃OCl proceeds with a room temperature rate constant of $(6.1 \pm 0.2) \times 10^{-11} \text{ cm}^3 \text{ molecule}^{-1} \text{ s}^{-1}$. At the same temperature, chlorine abstraction dominates product formation (ca. 80%) with only a ca. 20% contribution from H atom abstraction. The fate of CH₃OCl in the polar stratosphere will be determined by competition between photolysis and reaction with Cl atoms. As most reactive encounters between Cl and CH₃OCl result in Cl₂ formation, both loss processes give essentially the same net conversion of O₃.

Acknowledgment. This work was funded in part by the CEC Project EV5V-CT93-0338, CABRIS, within the CEC Environment Programme.

References and Notes

- (1) Anderson, J. G.; Toohey, D. W.; Brune, W. H. *Science* **1991**, *251*, 39.
- (2) Solomon, S. *Nature* **1990**, *347*, 347.
- (3) Crutzen, P. J.; Müller, R.; Brühl, C.; Peter, T. *Geophys. Res. Lett.* **1992**, *19*, 1113.
- (4) Helleis, F.; Crowley, J. N.; Moortgat, G. K. *J. Phys. Chem.* **1993**, *97*, 11464.
- (5) Helleis, F.; Crowley, J. N.; Moortgat, G. K. *Geophys. Res. Lett.* **1994**, *21*, 1795.
- (6) Kenner, R. D.; Ryan, K. R.; Plumb, I. C. *Geophys. Res. Lett.* **1993**, *20*, 1571.
- (7) Kukui, A.; Jungkamp, T.; Schindler, R. N. *Ber. Bunsen-Ges. Phys. Chem.* **1994**, *98*, 1298.
- (8) Biggs, P.; Canosa-Mas, C. E.; Fracheboud, J. M.; Shallcross, D. E.; Wayne, R. P. *Geophys. Res. Lett.* **1995**, *22*, 1221.
- (9) Crowley, J. N.; Helleis, F.; Müller, R.; Moortgat, G. K.; Crutzen, P. J.; Orlando, J. J. *Geophys. Res.* **1994**, *99*, 20683.
- (10) Crowley, J. N.; Campuzano-Jost, P.; Moortgat, G. K. *J. Phys. Chem.* **1996**, *100*, 3601.
- (11) Benson, S. W. *Thermochemical Kinetics*; Wiley: New York, 1976.
- (12) DeMore, W. B.; Sander, S. P.; Golden, D. M.; Hampson, R. F.; Kurylo, M. J.; Howard, C. J.; Ravishankara, A. R.; Kolb, C. E.; Molina, M. J. *Chemical Kinetics and Photochemical Data for Use in Stratospheric Modeling*; JPL Publication 94-26; Pasadena, 1994.
- (13) Finkbeiner, M.; Neeb, P.; Horie, O.; Moortgat, G. K. *Fresenius J. Anal. Chem.* **1995**, *351*, 521.
- (14) Moortgat, G. K.; Cox, R. A.; Schuster, G.; Burrows, J. P.; Tyndall, G. S. *J. Chem. Soc., Faraday Trans. 2* **1989**, 809.
- (15) Raber, W.; Moortgat, G. K. In *Progress and Problems in Atmospheric Chemistry*; Barker, J. R., Ed.; World Scientific Press: Singapore, 1996; Vol. 3, pp 318–373.
- (16) Hsu, K. J.; DeMore, W. B. *J. Phys. Chem.* **1995**, *99*, 1235.
- (17) Su, F.; Calvert, J. G.; Shaw, J. S. *J. Phys. Chem.* **1979**, *25*, 3185.
- (18) Veyret, B.; Lesclaux, R.; Rayez, M.; Rayez, J.; Cox, R. A.; Moortgat, G. K. *J. Phys. Chem.* **1989**, *93*, 2368. Burrows, J. P.; Moortgat, G. K.; Tyndall, G. S.; Cox, R. A.; Jenkin, M. E.; Hayman, G. D.; Veyret, B. *J. Phys. Chem.* **1989**, *93*, 2375.
- (19) Su, F.; Calvert, J. G.; Shaw, J. H.; Niki, H.; Maker, P. D.; Savage, C. M.; Breitenbach, L. D. *Chem. Phys. Lett.* **1979**, *65*, 221.
- (20) Vaghjiani, G. L.; Ravishankara, A. R. *J. Phys. Chem.* **1989**, *93*, 1948.
- (21) Curtis, A. R.; Sweetenham, W. P. Facsimile program. AERE Report R-12805; HMSO: Londong, 1987.
- (22) Maric, D.; Burrows, J. P.; Meller, R.; Moortgat, G. K. *J. Photochem. Photobiol. A* **1993**, *70*, 205.
- (23) Meller, R. Diploma Thesis, University of Mainz, Germany, 1991 (data measured in this laboratory).
- (24) Libuda, H. G.; Zabel, F.; Fink, E. H.; Becker, K. H. *J. Phys. Chem.* **1990**, *94*, 5860.
- (25) Nielsen, O. J.; Sidebottom, H. W.; Donlon, M.; Treacy, J. *Chem. Phys. Lett.* **1991**, *178*, 163.
- (26) Nielsen, O. J.; Sidebottom, H. W.; Donlon, M.; Treacy, J. *Int. J. Chem. Kinet.* **1991**, *23*, 1095.
- (27) Kukui, A.; Benter, Th.; Schindler, R. N. Data presented at the 2nd Euroconference, "6th sensing the atmosphere", Marbella, Spain, 1996.
- (28) Müller, R.; Crutzen, P. J. *J. Geophys. Res.* **1993**, *98*, 20483.
- (29) Müller, R.; Peter, Th.; Crutzen, P. J.; Oelhaf, H.; Adrian, G. P.; Clarmann, Th. v.; Wegner, A.; Schmidt, U.; Lary, D. *Geophys. Res. Lett.* **1994**, *21*, 1427.
- (30) Müller, R.; Brenninkmeijer, C. A. M.; Crutzen, P. J. A large ¹³C deficit in the lower Antarctic stratosphere due to "ozone hole" chemistry: Part II Modelling (1996). *Geophys. Res. Lett.* **1996**, *23*, 2129.
- (31) Lary, D. J.; Pyle, J. A. *J. Atmos. Chem.* **1991**, *13*, 373.
- (32) Fahey, D. W.; Kelly, K. K.; Kawa, S. R.; Tuck, A. F.; Loewenstein, M.; Chun, K. R.; Heidt, L. E. *Nature* **1990**, *344*, 321.
- (33) Kelly, K. K.; Tuck, A. F.; Heidt, L. E.; Loewenstein, M.; Podolske, J. R.; Strahan, S. E.; Vedder, J. F. *Geophys. Res. Lett.* **1990**, *17*, 465.
- (34) Russell, J. M., III; Gordley, L. L.; Park, J. H.; Drayson, S. R.; Tuck, A. F.; Harries, J. E.; Cicerone, R. J.; Crutzen, P. J.; Frederick, J. E. *J. Geophys. Res.* **1993**, *98*, 10777.
- (35) Poole, L. R.; Pitts, M. C. *J. Geophys. Res.* **1994**, *99*, 13083.
- (36) Woodbridge, E. L.; Elkins, J. W.; Fahey, D. W.; Heidt, L. E.; Solomon, S.; Baring, T. J.; Gilpin, T. M.; Pollock, W. H.; Schaufli, S. M.; Atlas, E. L.; Loewenstein, M.; Podolske, J. R.; Webster, C. R.; May, R. D.; Gilligan, J. M.; Montzka, S. A.; Boering, K. A.; Salawich, R. J. *J. Geophys. Res.* **1995**, *100*, 3057.
- (37) Douglass, A. R.; Schoeberl, M. R.; Stolarski, R. S.; Waters, J. W.; Russell, J. M., III; Roche, A. E.; Massie, S. T. *J. Geophys. Res.* **1995**, *100*, 13967.

JP9611075